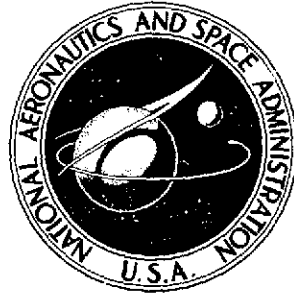


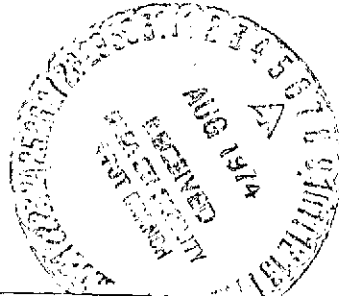
mid

NASA TECHNICAL NOTE



NASA TN D-7719

NASA TN D-7719



(NASA-TN-D-7719) ANALYSIS OF SOUND PROPAGATION IN DUCTS USING THE WAVE ENVELOPE CONCEPT (NASA) 40 p HC \$3.25	N74-29654
CSCL 20D	Unclas
	H1/12 54800

ANALYSIS OF SOUND PROPAGATION IN DUCTS USING THE WAVE ENVELOPE CONCEPT

by Kenneth J. Baumeister

Lewis Research Center

Cleveland, Ohio 44135



1. Report No. NASA TN D-7719	2. Government Accession No.	3. Recipient's Catalog No.	
4. Title and Subtitle ANALYSIS OF SOUND PROPAGATION IN DUCTS USING THE WAVE ENVELOPE CONCEPT		5. Report Date JULY 1974	6. Performing Organization Code
		8. Performing Organization Report No. E-7941	10. Work Unit No. 501-04
7. Author(s) Kenneth J. Baumeister		11. Contract or Grant No.	
9. Performing Organization Name and Address Lewis Research Center National Aeronautics and Space Administration Cleveland, Ohio 44135		13. Type of Report and Period Covered Technical Note	
		14. Sponsoring Agency Code	
12. Sponsoring Agency Name and Address National Aeronautics and Space Administration Washington, D.C. 20546		15. Supplementary Notes	
16. Abstract A finite difference formulation is presented for sound propagation in a rectangular two-dimensional duct without steady flow for plane wave input. Before the difference equations are formulated, the governing Helmholtz equation is first transformed to a form whose solution does not oscillate along the length of the duct. This transformation reduces the required number of grid points by an order of magnitude, and the number of grid points becomes independent of the sound frequency. Physically, the transformed pressure represents the amplitude of the conventional sound wave. Example solutions are presented for sound propagation in a one-dimensional straight hard-wall duct and in a two-dimensional straight soft-wall duct without steady flow. The numerical solutions show evidence of the existence along the duct wall of a developing "acoustic pressure diffusion boundary layer" which is similar in nature to the conventional viscous flow boundary layer. In order to better illustrate this concept, the wave equation and boundary conditions are written such that the frequency no longer appears explicitly in them. The frequency effects in duct propagation can be visualized solely as an expansion and stretching of the suppressor duct.			
17. Key Words (Suggested by Author(s)) Noise Duct Finite difference Boundary layer		18. Distribution Statement Unclassified - unlimited Category 12	
19. Security Classif. (of this report) Unclassified	20. Security Classif. (of this page) Unclassified	21. No. of Pages 38	22. Price* \$3.25

* For sale by the National Technical Information Service, Springfield, Virginia 22151

ANALYSIS OF SOUND PROPAGATION IN DUCTS USING

THE WAVE ENVELOPE CONCEPT

by Kenneth J. Baumeister

Lewis Research Center

SUMMARY

A finite difference formulation is presented for sound propagation in a rectangular two-dimensional duct without steady flow. In the numerical analysis, the continuous acoustic field is lumped into a series of grid points in which the pressure and velocity at each grid point are separated into real and imaginary parts. Before the difference equations are formulated, the governing Helmholtz equation is first transformed to a form whose solution does not oscillate along the length of the duct. The transformation is valid for problems in which a plane pressure wave is assumed to exist at the duct entrance. This transformation reduces the required number of grid points by an order of magnitude, and the number of grid points becomes independent of the sound frequency.

Physically, the transformed pressure represents the amplitude of the conventional sound wave. Example solutions are presented for sound propagation in a one-dimensional straight hard-wall duct and in a two-dimensional straight soft-wall duct without steady flow. These numerical solutions are in good agreement with the exact analytical results. The numerical solution shows evidence of the existence along the duct wall of a developing "acoustic pressure diffusion boundary layer" which is similar in nature to the conventional viscous flow boundary layer. In order to better illustrate this concept, the wave equation and boundary conditions are written such that the frequency no longer appears explicitly in them. The frequency effects in duct propagation can be visualized solely as an expansion and stretching of the suppressor duct.

INTRODUCTION

The level of noise regulations currently being proposed for new aircraft requires the use of acoustic suppression in the inlet and exhaust ducts of their engines. For suppressor ducts of infinite length and uniform area, flow, impedance, and so forth, analytical

methods (refs. 1 to 18) have been successfully applied. The analytical methods use the technique of separation of variables to obtain a complex eigenvalue formulation in which the eigenvalues are determined by various numerical techniques. The analytical techniques, however, become difficult to apply to the more complex acoustic transmission problems in ducts which are nonuniform due to variations in axial area and flow (refs. 19 to 23).

The numerical difference technique is an attractive alternative to the analytical techniques for complex acoustic liner design problems which consider area variations, impedance changes along the duct, and large flow gradients. In references 24 to 26, the numerical difference technique has been applied to the problems of sound propagation in two-dimensional straight hard- and soft-wall ducts with and without steady flow. However, the full potential of the application of the finite difference technique to the more complex problems mentioned has not yet been realized.

In the numerical analysis, the continuous acoustic field is lumped into a series of grid points in which the pressure and velocity at each grid point are separated into real and imaginary parts. One of the principal reasons why the finite difference technique has not yet been applied to the more complex problems is the large computer storage requirements (ref. 24). Since the solution matrix for the acoustic flow field is not positive definite, conventional iteration techniques cannot be used to solve the difference equation. As stated in reference 24, before the finite difference formulation can be applied to more complicated problems which require a large number of grid points, iteration techniques or more efficient closed-form matrix solutions will have to be developed to overcome present grid-size limitations.

The work reported herein was conducted to reduce the number of grid points necessary to solve a given problem by the finite difference technique. This reduction is accomplished by the use of a spatial transformation of the sound pressure. First, the governing acoustic wave equation is transformed to a new form whose solution eliminates the usual acoustic sound pressure oscillations which occur in the axial direction along the duct. This transformation is accomplished by using the well-known analytical solution for pressure propagation in a hard-wall duct as a base for the complete solution. The transformation is used for problems in which a plane pressure wave is assumed to exist at the duct entrance.

If the inlet pressure profile is in the form of a high-order radial mode rather than a plane wave, the transformation used for plane wave propagation may not be appropriate or advantageous. For such cases, an extension of the transformation technique to a wider class of initial conditions is presented in an appendix of this report.

WAVE ENVELOPE CONCEPT

This section reviews the previously published (refs. 24 to 26) finite difference theory and shows how this past work suggests the transformation which is applied to the governing equations.

Wave Equation

The operation of a typical turbojet suppressor using (for example) a Helmholtz resonator as a noise absorber is shown schematically in figure 1. The noise source shown in figure 1 has associated with it some initial pressure profile and some entering acoustic energy flux represented by the symbol I' (intensity). The entering acoustic energy is dissipated along the length of the duct by viscous action within and associated with the Helmholtz absorbers imbedded in the walls of the duct. The acoustic particle fluid velocities u'_x and u'_y shown in figure 1 play an important role in the dissipation process as well as in the transmission of the acoustic energy along the duct.

The governing equation describing the propagation of acoustic energy is the wave equation. The two-dimensional form of the wave equation without steady flow is given by

$$\frac{\partial^2 P'}{\partial x'^2} + \frac{\partial^2 P'}{\partial y'^2} = \frac{1}{c^2} \frac{\partial^2 P'}{\partial t^2} \quad (1)$$

In this equation, the prime is used to denote a dimensional quantity. These and all other symbols used in the report are defined in appendix A.

As customary for steady state, the solution for the pressure is assumed to be of the complex form

$$P'(x', y', t) = P'_0(x', y') e^{i\omega t} \quad (2)$$

The final solution for pressure is represented by the real part of this complex representation of the pressure. Substitution of equation (2) into equation (1) and introduction of the following dimensionless parameters

$$P = \frac{P'_0}{P'_A} \quad (3)$$

$$\left. \begin{aligned} x &= \frac{x'}{H} \\ y &= \frac{y'}{H} \end{aligned} \right\} \quad (4)$$

yield the classic Helmholtz equation

$$\frac{\partial^2 P}{\partial x^2} + \frac{\partial^2 P}{\partial y^2} + (2\pi\eta)^2 P = 0 \quad (5)$$

where the dimensionless frequency η is given as

$$\eta = \frac{H}{2\pi} \frac{\omega}{c} = \frac{Hf}{c} = \frac{H}{\lambda} \quad (6)$$

The frequency parameter η represents the ratio of duct height H to acoustic axial wavelength λ for the geometry shown in figure 1.

Figure 2 represents the same duct in dimensionless coordinates. The dimensionless transverse coordinate y ranges from zero to 1 while the dimensionless axial coordinate (length) x ranges from zero to L/H . The dimensionless pressure P has in general both real and imaginary parts; thus,

$$P(x, y) = P^{(1)}(x, y) + iP^{(2)}(x, y) \quad (7)$$

Consequently, equation (5) can be broken into its real and imaginary parts by substituting equation (7) into equation (5),

$$\frac{\partial^2 P^{(1)}}{\partial x^2} + \frac{\partial^2 P^{(1)}}{\partial y^2} + (2\pi\eta)^2 P^{(1)} = 0 \quad (8)$$

$$\frac{\partial^2 P^{(2)}}{\partial x^2} + \frac{\partial^2 P^{(2)}}{\partial y^2} + (2\pi\eta)^2 P^{(2)} = 0 \quad (9)$$

For simplicity, these two equations can be represented as a single equation

$$\frac{\partial^2 P^{(J)}}{\partial x^2} + \frac{\partial^2 P^{(J)}}{\partial y^2} + (2\pi\eta)^2 P^{(J)} = 0 \quad (10)$$

where J equals 1 or 2. Now, the solution of equation (10) will be investigated for the simple case of a plane pressure wave propagating in a hard-wall duct. From this simple example, a transformation of equation (5) will logically follow.

Hard-Wall Duct

Consider the propagation of a plane pressure wave into a hard-wall duct of length $x = L/H$ with a ρc exit impedance. The ρc exit impedance results in an absence of reflected waves; thus, the transverse pressure profiles are the same as in an infinite duct. For hard walls, the transverse pressure gradient is zero. Therefore, for one-dimensional sound propagation in the x -direction, the dimensionless wave equation (5) reduces to

$$\frac{\partial^2 P}{\partial x^2} + (2\pi\eta)^2 P = 0 \quad (11)$$

For an initial amplitude wave of unity

$$P = 1 \quad \text{at } x = 0 \quad (12)$$

and an exit impedance

$$Z = \rho c \quad \text{at any } x > 0 \quad (13)$$

the solution for the spatial pressure P is readily found analytically by a closed-form integration of equation (11) to be (see any acoustic text or appendix B of ref. 24)

$$P = e^{-i2\pi\eta x} \quad (14)$$

or

$$P = \cos 2\pi\eta x - i \sin 2\pi\eta x \quad (15)$$

Thus, in terms of the real and imaginary pressures which are used in the numerical solutions

$$P^{(1)} = \cos 2\pi\eta x \quad (16)$$

$$P^{(2)} = -\sin 2\pi\eta x \quad (17)$$

Numerically, the same results can be found by finite difference solution of equation (10). In appendix B of reference 24, the pressure profile associated with a hard-wall finite-length duct with a ρc exit impedance (eqs. (16) and (17)) is shown to be identical to that of an infinitely long duct with no reflected waves.

Finite Difference Grid Spacing

As was mentioned in the INTRODUCTION, in a finite difference numerical analysis, the continuous acoustic field is lumped into a series of grid points in which the pressure at each point is separated into real and imaginary parts. The grid points for the hard-wall-duct problem are shown in the sketch in figure 3. As mentioned earlier, because there is no variation of pressure in the y -direction in the hard-wall duct, the general two-dimensional grid lattice (fig. 4) can be reduced to a one-dimensional lattice as shown in the sketch in figure 3.

In reference 24, the numerical and analytical values of the pressure were computed for the special case of a hard-wall duct with an L/H of 1 and an inlet plane wave with a dimensionless frequency η equal to 1. The analytical and numerical values of the acoustic pressure profiles along the duct are shown in figure 3. The pressures calculated at the finite difference grid points by the numerical finite difference technique are shown by the square symbols on the graph. As seen in figure 3, the agreement between the numerical and analytical results is good.

By a series of numerical calculations, the number of grid points necessary to get pressure profiles, velocities, and intensities accurate to about 4 percent was found to be (ref. 24)

$$n \approx 12\eta \left(\frac{L}{H} \right) \quad (18)$$

Thus, for the unit frequency ($\eta = 1$) and unit length ($L/H = 1$) shown in figure 3, about 12 grid points were necessary to describe adequately the sinusoidal form of the spatial pressure dependence. If the frequency is doubled ($\eta = 2$), clearly twice as many points

(24 points) will be required to describe the wave. For the general two-dimensional problem in which pressure gradients exist in the y -direction, the total number of grid points becomes

$$(\text{Total number of grid points}) = m \times n = 12m\eta \left(\frac{L}{H} \right) \quad (19)$$

where m represents the number of grid points in a column in the transverse direction, as shown in figure 4 for a two-dimensional grid. A value of $m = 10$ was found to be sufficient. Clearly, as discussed in the INTRODUCTION, large values of $\eta(Hf/c)$ or L/H greatly increase the computer storage and running time.

Soft-Wall Duct

In a soft-wall suppressor the amplitude of $P^{(1)}$ and $P^{(2)}$ decreases in the axial direction down the length of the duct because of acoustic energy dissipation at the wall. This observation is shown in figure 5. However, the basic axial variation of the pressure wave is similar to that in a hard-wall duct. Thus, the number of grid points in the axial direction still depends on frequency η and dimensionless duct length L/H , as shown in equation (18).

Next, a concept is considered which eliminates the dependency of the total number of grid points on η and L/H .

Envelope Transformation

Consider the example case of a soft-wall duct with an L/H of 3 and an inlet plane wave with a dimensionless frequency η equal to 1. A typical $P^{(1)}$ pressure profile in a suppressor duct is shown in figure 6 by the heavy solid line, while the dashed lines represent the envelope of the solid pressure wave amplitude. From equation (18), the number of grid points n needed should be about 36. However, if the basic Helmholtz equation (5) could be transformed so that it would describe the envelope (dashed lines) of the pressure rather than the pressure wave itself, the 36-point requirement could be greatly reduced. As shown in figure 6, five points are used to describe the pressure envelope.

The assumption is now made that the spatial pressure $P(x, y)$ can be separated into two parts as follows:

$$P(x, y) = p(x, y)f(x) \quad (20)$$

where $f(x)$ represents the term which accounts for axial oscillations and $p(x,y)$ represents the amplitude of the oscillations. For the problems with a uniform pressure wave entering a soft-wall duct to be considered herein, the analytical solution for pressure propagation in a hard-wall duct is used for $f(x)$. Thus, from equation (14)

$$f(x) = e^{-i2\pi\eta x} \quad (21)$$

or since f can also be broken into its real and imaginary parts

$$f = f^{(1)} + if^{(2)} \quad (22)$$

Thus,

$$f^{(1)} = \cos 2\pi\eta x \quad (23)$$

and

$$f^{(2)} = -\sin 2\pi\eta x \quad (24)$$

The utility of the assumed form of $f(x)$ rests on the numerical solution for $p(x,y)$ being a smoothly varying function.

The analytical theory (ref. 3) indicates that if the inlet pressure profile is in the form of a higher order radial mode rather than a plane wave, or if two or more higher order radial modes propagate through the duct (cut on), the axial propagation wavelength may be considerably different from the wavelength associated with hard-wall-duct propagation as given by equation (21). In this case, the assumed form of $f(x)$ could lead to large ripples in the solution for $p(x)$. Although the governing differential equation is valid even if ripples are present, a sparse axial grid system will no longer produce accurate predictions of pressure and acoustic intensity. However, for such cases, an extension of the transformation technique to a wider class of initial conditions is presented in appendix B.

Next, equations (20) and (24) are used to establish the transformed form of the governing equations and boundary conditions.

TRANSFORMED EQUATIONS AND BOUNDARY CONDITIONS

The governing differential equation and boundary conditions are introduced in this section of the report. The boundary conditions are first presented in dimensional form and then made dimensionless.

Transformed Acoustic Pressure Field

The Helmholtz equation (5) represents the governing equation for pressure in the duct. Substitution of equations (20) and (21) into equation (5) yields the governing equation

$$\frac{\partial^2 p}{\partial x^2} + \frac{\partial^2 p}{\partial y^2} - i4\pi\eta \frac{\partial p}{\partial x} = 0 \quad (25)$$

Just as with the pressure P , the dimensionless pressure p has in general both real and imaginary parts. Thus,

$$p(x, y) = p^{(1)}(x, y) + ip^{(2)}(x, y) \quad (26)$$

Consequently, equation (25) can be broken into its real and imaginary parts by substituting equation (26) into equation (25),

$$\frac{\partial^2 p^{(1)}}{\partial x^2} + \frac{\partial^2 p^{(1)}}{\partial y^2} + 4\pi\eta \frac{\partial p^{(2)}}{\partial x} = 0 \quad (27)$$

$$\frac{\partial^2 p^{(2)}}{\partial x^2} + \frac{\partial^2 p^{(2)}}{\partial y^2} - 4\pi\eta \frac{\partial p^{(1)}}{\partial x} = 0 \quad (28)$$

For simplicity, these two equations can be represented as a single equation

$$\frac{\partial^2 p^{(J)}}{\partial x^2} + \frac{\partial^2 p^{(J)}}{\partial y^2} - (-1)^J 4\pi\eta \frac{\partial p^{(K)}}{\partial x} = 0 \quad (29)$$

where J equals 1 or 2 and K equals 2 or 1, respectively.

The two equations represented by equation (29) are the basic governing equations for noise propagation which are solved later in this report by a difference formulation. As can be seen in equation (29), the real component of p , $p^{(1)}$, is coupled to the imaginary part $p^{(2)}$ through the term containing the dimensionless frequency η . Recall that in the Helmholtz equation (5) the real and imaginary terms are not coupled in the governing equation. The $P^{(1)}$ and $P^{(2)}$ pressures, however, are coupled in the boundary condition as is also the case for the transformed pressures $p^{(1)}$ and $p^{(2)}$.

Acoustic Particle Velocity

The boundary conditions in acoustics are generally given in terms of impedances which relate the pressure and velocity fields at the boundary. For no mean flow, the acoustic velocity field can be expressed in terms of pressure from the momentum equation

$$\rho \left(\frac{\partial \bar{\mathbf{u}}'}{\partial t} \right) = -\nabla' P' \quad (30)$$

which for a harmonic solution of the form given by equation (2) reduces to

$$\bar{\mathbf{u}}' = \frac{i}{\rho \omega} \nabla' P' \quad (31)$$

In terms of the velocities, equation (31) becomes

$$u'_x = \frac{i}{\rho \omega} \frac{\partial P'}{\partial x'} \quad (32)$$

$$u'_y = \frac{i}{\rho \omega} \frac{\partial P'}{\partial y'} \quad (33)$$

In terms of the dimensionless parameters, equations (32) and (33) become

$$u_x = i \frac{\partial P}{\partial x} \quad (34)$$

$$u_y = i \frac{\partial P}{\partial y} \quad (35)$$

where

$$\bar{\mathbf{u}} = \frac{\rho \omega H}{P_A} \bar{\mathbf{u}}' \quad (36)$$

These velocities expressed in terms of the transformed pressure become

$$u_x = \left(2\pi\eta p + i \frac{\partial p}{\partial x} \right) e^{-i2\pi\eta x} \quad (37)$$

$$u_y = ie^{-i2\pi\eta x} \frac{\partial p}{\partial y} \quad (38)$$

Impedance Boundary Condition

In the transverse direction, the acoustic impedance at the walls is defined as

$$Z = \frac{P'}{u_y'} \quad \text{at } y = 0 \text{ and } 1 \quad (39)$$

The impedance Z is now replaced by the impedance ratio ζ , which is defined as

$$\zeta = \frac{Z}{\rho c} = \theta + i\chi \quad (40)$$

Substituting equation (33) into equation (39) and introducing the dimensionless parameters yield the following expression for the impedance ratio at the walls:

$$\zeta = -i2\pi\eta \frac{P}{\left(\frac{\partial P}{\partial y}\right)} \quad \text{at } y = 0 \text{ and } 1 \quad (41)$$

Or the pressure gradients at the walls becomes

$$\frac{\partial P}{\partial y} = \frac{-i2\pi\eta}{\zeta} P \quad \text{at } y = 0 \text{ and } 1 \quad (42)$$

It is convenient to express the reciprocal of the impedance ratio in terms of the acoustic conductance ratio κ and the acoustic susceptance ratio σ ; that is,

$$\frac{1}{\zeta} \equiv \kappa - i\sigma \quad (43)$$

where $1/\zeta$ is called the acoustic admittance ratio. Therefore, equation (42) becomes

$$\frac{\partial P}{\partial y} = -2\pi\eta(\sigma + i\kappa)P \quad (44)$$

Substituting the expression for the transformed pressure (eq. (20)) yields

$$\frac{\partial p}{\partial y} = -2\pi\eta(\sigma + i\kappa)p \quad (45)$$

which is the same form as equation (44). Finally, expressing equation (45) in terms of its real and imaginary parts gives

$$\frac{\partial p^{(J)}}{\partial y} = -2\pi\eta \left[p^{(J)} \sigma + (-1)^J p^{(K)} \kappa \right] \quad \text{at } y = 0 \text{ and } 1 \quad (46)$$

Exit Boundary Condition

The exit condition to be presented now allows the numerical solutions to be compared to the analytical results for wave propagation in an infinitely long duct. The entrance region of length L in an infinitely long duct with uniform impedance will not have reflections at any position in the duct. The wave propagation in the entrance region of the infinite duct can be represented with a finite length of duct L by closing the exit impedance at L so that no reflections occur. Consequently, if the exit condition in the numerical analysis is chosen to eliminate reflections at the exit of the duct, the numerical and analytical results should be in close agreement.

The exit impedance is defined as

$$Z(x, y) = \frac{P'}{u'_x} \quad \text{at } x = L \quad (47)$$

For a plane wave propagating in a hard-wall duct, the condition for no reflections at the duct exit is an exit impedance of ρc . The ρc exit impedance is now used as the exit impedance for the soft-wall duct. This assumed exit condition was used and tested in reference 24 and shown to give good agreement between the numerical and analytical results. Substitution of ρc for Z in equation (47) gives, after some algebraic manipulations,

$$\frac{\partial P}{\partial x} = -i2\pi\eta P \quad (48)$$

Equation (48) can be expressed in terms of the transformed pressure by substituting equations (20) and (21) into equation (47). This yields

or

$$\left. \begin{aligned} \frac{\partial p}{\partial x} &= 0 \\ \frac{\partial p^{(J)}}{\partial x} &= 0 \end{aligned} \right\} \quad (49)$$

The zero slope reflects the assumption of a uniform ρc exit impedance.

Entrance Conditions

For the entrance pressure profile, the assumption used by Rice (ref. 3) of a uniform profile is used herein. This assumption is compatible with the assumed transformation parameter $f(x)$ defined in equation (2). For a uniform pressure profile,

and

$$\left. \begin{aligned} p^{(1)}(0, y) &= 1 \\ p^{(2)}(0, y) &= 0 \end{aligned} \right\} \quad (50)$$

in terms of the transformed pressure

and

$$\left. \begin{aligned} p^{(1)}(0, y) &= 1 \\ p^{(2)}(0, y) &= 0 \end{aligned} \right\} \quad (51)$$

Axial Acoustic Power

The sound power which leaves a duct and reaches the far field is related to the axial intensity. The axial intensity can be expressed as

$$I' = \frac{1}{2} \operatorname{Re} (P^* u'_x) \quad (52)$$

or in terms of the dimensionless parameters, equation (52) can be written in dimensionless form as

$$I = \frac{1}{2\pi\eta} \rho c (P^* u_x) \quad (53)$$

where

$$I = \frac{2\rho c}{P_A^2} I' \quad (54)$$

For a hard-wall duct with a ρc exit impedance, I is identical to 1 for all frequencies and duct lengths (see appendix B of ref. 24).

In terms of the complex representation, the expression for I becomes

$$I = \frac{1}{2\pi\eta} \left[P^{(2)} \frac{\partial P^{(1)}}{\partial x} - P^{(1)} \frac{\partial P^{(2)}}{\partial x} \right] \quad (55)$$

Expression $P^{(1)}$ and $P^{(2)}$ in terms of the transformed pressures $p^{(1)}$ and $p^{(2)}$ yields

$$I = p^{(1)2} + p^{(2)2} + \frac{1}{2\pi\eta} \left[p^{(2)} \frac{\partial p^{(1)}}{\partial x} - p^{(1)} \frac{\partial p^{(2)}}{\partial x} \right] \quad (56)$$

The total dimensionless acoustic power is the integral of the intensity across the test section

$$E_x = \int_0^1 I(x, y) dy \quad (57)$$

By definition the decrease in decibels of the acoustic power from 0 to x can be written as

$$\Delta dB = 10 \log_{10} \left(\frac{E_x}{E_0} \right) \quad (58)$$

FINITE DIFFERENCE FORMULATION

The continuous system is now reduced to an equivalent lumped-parameter system by means of a finite difference approximation. Instead of a continuous solution for the pressure, it is determined at the isolated grid points as shown in figure 4.

For problems where the gradient is specified at a boundary, such as in our acoustic problem, the integration method for generating the finite difference approximation is convenient to use. The basic difference equations are determined by integrating the approximate differential equation over a unit cell, as shown in figure 7. The cell is enclosed by the dashed lines which are spaced midway between the grid lines (not shown). The grid lines would go directly through the grid points. Thus, the integration of equation (29) over the cell becomes

$$\iint_{\text{cell}} \left[\nabla^2 p^{(J)} - (-1)^J 4\pi\eta \frac{\partial p^{(K)}}{\partial x} \right] dA = 0 \quad (59)$$

By applying Green's theorem for the plane region, equation (59) becomes

$$\oint \frac{\partial p^{(J)}}{\partial N} dS - (-1)^J 4\pi\eta \iint_{\text{cell}} \frac{\partial p^{(K)}}{\partial x} dA = 0 \quad (60)$$

where dA is a differential area element of the unit cell, dS is the differential length on the boundary of the unit cell, and N is the outward normal to the cell boundary.

As usual, the difference formulation approximates the first derivatives as follows:

$$\left. \frac{\partial p}{\partial x} \right|_{i+\frac{1}{2},j} = \frac{p_{i+1,j} - p_{i,j}}{\Delta x} \quad (61)$$

$$\left. \frac{\partial p}{\partial x} \right|_{i-\frac{1}{2},j} = \frac{p_{i,j} - p_{i-1,j}}{\Delta x} \quad (62)$$

$$\left. \frac{\partial p}{\partial x} \right|_{i,j} = \frac{p_{i+1,j} - p_{i-1,j}}{2 \Delta x} \quad (63)$$

$$\left. \frac{\partial p}{\partial y} \right|_{i,j+\frac{1}{2}} = \frac{p_{i,j+1} - p_{i,j}}{\Delta y} \quad (64)$$

and so forth.

Difference Equations

Cell 1 - central. - The integration equation (60) is now applied to the central region of the duct, labeled cell 1 in figure 7. In evaluating the surface integrals in equation (60), the gradients are assumed to be constant on each side of the cell, and the interior pressure gradient is evaluated at the average pressure gradient over the cell; that is,

$$\iint_{\text{cell}} \frac{\partial p^{(K)}}{\partial x} dA = \overline{\frac{\partial p^{(K)}}{\partial x}} \iint_{\text{cell}} dA \quad (65)$$

Thus, equation (60) becomes

$$\begin{aligned} -p_{i-1,j}^{(J)} - \left(\frac{\Delta x}{\Delta y}\right)^2 p_{i,j-1}^{(J)} + 2 \left[1 + \left(\frac{\Delta x}{\Delta y}\right)^2 \right] p_{i,j}^{(J)} - p_{i+1,j}^{(J)} - \left(\frac{\Delta x}{\Delta y}\right)^2 p_{i,j+1}^{(J)} \\ - (-1)^J 2\pi\eta \Delta x p_{i-1,j}^{(K)} + (-1)^J 2\pi\eta \Delta x p_{i+1,j}^{(K)} = 0 \end{aligned} \quad (66)$$

For a difference equation very similar to equation (66), some intermediate algebraic steps involved in the derivation are presented in appendixes C and D of reference 24.

Cell 2 - wall. - Now consider the difference equation which applies in cell 2, which is adjacent to the upper boundary in figure 7. For this unit cell, equation (60) can be expressed as

$$\begin{aligned} -\frac{1}{2} p_{i-1,m}^{(J)} - \left(\frac{\Delta x}{\Delta y}\right)^2 p_{i,m-1}^{(J)} + \left[1 + \left(\frac{\Delta x}{\Delta y}\right)^2 + 2\pi\eta \frac{\Delta x^2}{\Delta y} \sigma \right] p_{i,m}^{(J)} - \frac{1}{2} p_{i+1,m}^{(J)} \\ - (-1)^J \pi\eta \Delta x p_{i-1,m}^{(K)} + (-1)^J 2\pi\eta \frac{\Delta x^2}{\Delta y} \kappa p_{i,m}^{(K)} + (-1)^J \pi\eta \Delta x p_{i+1,m}^{(K)} = 0 \end{aligned} \quad (67)$$

where equation (46) was used to evaluate $\partial p^{(J)}/\partial y$ along the wall. A similar equation applies at the lower wall.

Cell 3 - exit. - In a similar manner, the difference equation which applies to cell 3 is found to be

$$\begin{aligned}
& -p_{n-1,j}^{(J)} - \frac{1}{2} \left(\frac{\Delta x}{\Delta y} \right)^2 p_{n,j-1}^{(J)} + \left[1 + \left(\frac{\Delta x}{\Delta y} \right)^2 \right] p_{n,j}^{(J)} - \frac{1}{2} \left(\frac{\Delta x}{\Delta y} \right)^2 p_{n,j+1}^{(J)} \\
& - (-1)^J 2\pi\eta \Delta x p_{n-1,j}^{(K)} + (-1)^J 2\pi\eta \Delta x p_{n,j}^{(K)} = 0 \quad (68)
\end{aligned}$$

where equation (49) is used to evaluate $\partial p^{(J)}/\partial x$ at the exit.

Cell 4 - corner. - Finally, the difference equation for cell 4 is

$$\begin{aligned}
& -\frac{1}{2} p_{n-1,m}^{(J)} - \frac{1}{2} \left(\frac{\Delta x}{\Delta y} \right)^2 p_{n,m-1}^{(J)} + \frac{1}{2} \left[1 + \left(\frac{\Delta x}{\Delta y} \right)^2 + 2\pi\eta \frac{\Delta x^2}{\Delta y} \sigma \right] p_{n,m}^{(J)} \\
& - (-1)^J \pi\eta \Delta x p_{n-1,m}^{(K)} + (-1)^J \left(\pi\eta \frac{\Delta x^2}{\Delta y} \kappa + \pi\eta \Delta x \right) p_{n,m}^{(K)} = 0 \quad (69)
\end{aligned}$$

Axial Intensity

The axial intensity I was evaluated from equation (56) by using the following four-point differentiation formula (ref. 27)

$$\left. \frac{\partial p}{\partial x} \right|_i = \frac{1}{6 \Delta x} (-11p_i + 18p_{i+1} - 9p_{i+2} + 2p_{i+3}) \quad (70)$$

for the points adjacent to the boundaries and

$$\left. \frac{\partial p}{\partial x} \right|_i = \frac{1}{12 \Delta x} (p_{i-2} - 8p_{i-1} + 8p_{i+1} - p_{i+2}) \quad (71)$$

for central points.

The total intensity across the test section, as given by equation (57), is written in difference form as

$$E_i = \left[\frac{1}{2} I_{i,1} + \sum_{j=2}^{m-1} I_{i,j} + \frac{1}{2} I_{i,m} \right] \Delta y \quad (72)$$

We shall now apply the difference equations to the problem of noise attenuation in a duct.

MATRIX SOLUTIONS

The collection of the various difference equations at each grid point forms a set of simultaneous equations which can be expressed in matrix notation as

$$\{A\} \cdot [\bar{p}] = [\bar{F}] \quad (73)$$

where $\{A\}$ is the known coefficient matrix, $[\bar{p}]$ is the unknown column vector containing the unknown pressures, and $[\bar{F}]$ is the known column vector containing the various initial conditions, where $\{A\}$, $[\bar{p}]$, and $[\bar{F}]$ are complex in general.

Equation (73) can also be expressed in terms of all real quantities. In order to accomplish this, the column vector $[\bar{p}]$ is written in terms of $p^{(1)}$ and $p^{(2)}$ and the $\{A\}$ matrix is subdivided as follows

$$\left\{ \begin{array}{c|c} A_1 & -C \\ \hline +C & A_1 \end{array} \right\} \begin{bmatrix} \bar{p}^{(1)} \\ \bar{p}^{(2)} \end{bmatrix} = \begin{bmatrix} \bar{F}^{(1)} \\ \bar{F}^{(2)} \end{bmatrix} \quad (74)$$

Matrices of the form of equation (73) or (74) can be solved by elimination techniques. In particular, the Gauss elimination technique is used to find solutions of equation (74) in the example problems which follow. In this case, the computer storage limited the total grid points to 100. However, when a much larger number of grid points is required for a finite difference problem, a solution of the block tridiagonal form of the complex matrix equation (73) appears to be the most efficient from both operational time and computer storage considerations (personal communication from D. W. Quinn, Wright-Patterson Air Force Base, Dayton, Ohio).

EXAMPLE PROBLEMS

Two examples are presented to illustrate the numerical techniques. Both examples have analytical solutions; therefore, a direct comparison between the numerical and analytical techniques can be made. First, the simple case of plane waves propagating down a hard-wall duct is presented. This case allows comparison of the numerical and analytical pressure profiles down the length of the duct. The second example compares the numerical and analytical predictions of the attenuation in a soft-wall two-dimensional duct.

One-Dimensional Hard-Wall Duct

Numerical and analytical values of the pressure were computed for the special case of a hard-wall duct with a ρc exit impedance. The calculation was made for a duct with an L/H of 1 and an inlet plane wave with a dimensionless frequency η equal to 1. The analytical and numerical values of the acoustic pressure profiles $p(x)$ along the duct are shown in figure 8. Because there are no variations of pressure in the y -direction for hard walls, the pressure profiles shown in figure 8 apply at any value of y in the duct. As shown in figure 8, the agreement between the numerical and analytical results is good.

The dimensionless intensity I for a hard-wall duct is unity. For the pressure profiles shown in figure 8, $p^{(1)}$ has a value of unity, $p^{(2)}$ is zero, and the gradients of both $p^{(1)}$ and $p^{(2)}$ are zero. Thus, the value of intensity found from equation (56) is identical to 1, as expected.

A comparison with figure 3 indicates the essential differences between the transformed numerical solution and the conventional numerical solution for the same problem.

Two-Dimensional Soft-Wall Duct

Maximum attenuation. - As another example of the finite difference formulation, the noise attenuation at the optimum point (point of maximum attenuation in the impedance plane) is now calculated for a two-dimensional duct with L/H values ranging between 0.5 and 6 and input waves with dimensionless frequencies $\eta = Hf/c$ of 1, 2, and 5. This range of dimensionless parameters essentially covers the practical range of application to turbojet suppressors. For a uniform inlet pressure profile the analytical result shows that the values of specific acoustic impedance ζ associated with the optimum point are a function of these η and L/H values; that is, $\zeta_{\text{opt}} = f(\eta, L/H)$. The values of the optimum impedance used in the numerical analysis were determined from the analytical techniques presented in references 3 and 15.

The numerically calculated attenuations are compared to corresponding analytical results (refs. 3 and 15) which are applicable to infinite ducts. The numerical results (lines) and the analytical results (symbols) for the maximum attenuation are shown in figure 9. The analytical and numerical results are in very good agreement.

Based on the wave envelope concept, the numerical calculations shown in figure 9 used 10 grid columns in the axial direction. For $\eta = 5$ and $L/H = 6$, the standard finite difference technique required 360 grid columns, according to equation (18). Thus, for an $m = 10$, the total number of grid points has been reduced from 3600 to 100 when the wave envelope concept is employed. Since the computer computation time is proportional to the number of grid points cubed, this decrease in grid points represents a considerable time savings.

Acoustic pressure profiles. - Next consider the problem of a plane wave of dimensionless frequency $\eta = 1$ entering a soft-wall duct of length $L/H = 1$ and the impedance set at the optimum point. For this case, the transformed axial pressure amplitude profiles at various y -positions are shown in the upper portion of figure 10. The transverse pressure amplitude profiles along the duct are shown in the lower portion of figure 10. Near the wall ($y = 0$) the pressure amplitude remains near unity along most of the duct due to the action of the impedance condition at the wall. Also, as shown in figure 10, this pressure amplitude along the centerline remains near its hard-wall value at least halfway down the duct. Thus, the pressure at the centerline is "unaware" of the soft absorbing wall until halfway down the duct.

This phenomenon is analogous to the problem of a developing laminar velocity profile in the entrance region of a pipe. It takes a prescribed length down the pipe before the growing laminar boundary layers at the walls meet in the center of the pipe to establish the fully developed parabolic laminar flow profile. In sound propagation in ducts, it appears that a similar "acoustic pressure diffusion boundary layer" is being formed at the walls and that it takes a prescribed distance down the duct before the acoustic pressure diffusion boundary layers meet. If the height of the acoustic boundary layer is defined as the point where the pressure drops from 1 to a value of 0.95, the boundary layer growth is shown by the dashed lines in the lower portion of figure 10.

In the entrance region of a pipe with viscous laminar flow, the flow energy is lost through energy dissipation in the boundary layer near the wall. However, for the analogous idealized (no viscosity) acoustic problem, the viscous dissipation takes place outside the flow field inside the walls of the duct.

Effective frequency. - The question may logically be asked, how does the frequency of the sound affect the acoustic pressure diffusion boundary layer growth? To answer this question, the basic governing differential Helmholtz equation (5) is rewritten as

$$\frac{1}{\eta^2} \frac{\partial^2 P}{\partial x^2} + \frac{1}{\eta^2} \frac{\partial^2 P}{\partial y^2} + (2\pi)^2 P = 0 \quad (75)$$

These dimensionless forms were convenient in solving the problem; however, other choices could have been made. Now, let us define the new distance coordinates as

$$X = \eta x = \eta \frac{x'}{H} = \frac{x' f}{c} \quad (76)$$

$$Y = \eta y = \frac{y' f}{c} \quad (77)$$

For $y' = H$, that is, at the upper surface of the duct,

$$Y = \eta = \frac{Hf}{c} \quad \text{at upper surface} \quad (78)$$

and at the exit

$$X = \eta \frac{L}{H} = \frac{Lf}{c} \quad (79)$$

With the new length coordinates, the governing Helmholtz equation (75) takes on the form

$$\frac{\partial^2 P}{\partial X^2} + \frac{\partial^2 P}{\partial Y^2} + (2\pi)^2 P = 0 \quad (80)$$

In a similar manner, the impedance boundary condition (42) can also be expressed in terms of the new length scales as

$$\frac{\partial p}{\partial Y} = -i \frac{2\pi}{\xi} P \quad \text{at } Y = 0 \text{ and } Y = \eta \quad (81)$$

The frequency η no longer appears explicitly in the differential wave equation or boundary condition. Now, the frequency enters the problem through the limits of integration. Clearly, the dimensionless frequency can be visualized solely as an expansion and stretching of the suppressor duct as defined by equations (78) and (79). This is illustrated in figure 11. At higher frequencies, the acoustic pressure diffusion boundary layer does not penetrate into the larger duct fast enough to remove the acoustic energy. Thus, as shown in figure 9, the attenuation of the suppressor ducts decreases at higher frequencies.

Figure 12 displays the effects of higher frequency in a duct on the pressure profiles and the acoustic pressure diffusion boundary layer. Figure 12(a) considers the case of $\eta = 5$ and $L/H = 1$, while figure 12(b) considers the case of $\eta = 5$ and $L/H = 5$. A direct comparison can be made between the pressure profiles for the $\eta = 5$ case in figure 12(a) and the $\eta = 1$ case in figure 10. For the $\eta = 5$ case, as shown in figure 11, the effective height of the duct is much larger. As a result, as shown in figure 12(a), the pressure at the centerline is unaffected by the presence of a soft-wall absorber at the boundary until some value of L/H greater than 1. The pressures in the center of the duct remain at their initial or undisturbed value for much longer distances. This is reflected by the lower noise attenuation as displayed in figure 9 for higher η . Figure 12(b)

shows that for $\eta = 5$ the acoustic pressure diffusion boundary layer reaches the center of the duct at an L/H of about 2.

From figure 11, the requirement for equal grid resolution indicates that the number of grid points m in the y -direction should be proportional to η . Unfortunately, the computer storage was insufficient to increase the number of grid points m the required amount. This may account for the oscillations in the calculated pressure amplitudes shown in figures 10 and 12. In the future, however, programming the matrix in complex form, as suggested by D. W. Quinn of Wright-Patterson Air Force Base, Dayton, Ohio, should handle the problem.

Finally, by defining the effective frequency η_{eff} as

$$\eta_{\text{eff}} = \eta \left(\frac{H}{L} \right) \quad (82)$$

as was shown in reference 4, the optimal attenuation can be correlated as a function of η_{eff} . This result is shown in figure 13. Similar curves can be obtained from Rice's results for circular ducts when $\Delta\text{dB}/(L/H)$ is plotted against η . With the use of the dimensionless axial coordinate

$$x_{\text{eff}} = x \left(\frac{H}{L} \right) \quad (83)$$

the boundary layer profiles and the pressure profiles become roughly similar for equal values of η_{eff} and x_{eff} . This similarity can be seen by a comparison of the boundary layer and pressure profiles of figures 10 and 12(b). In these figures, both x_{eff} and η_{eff} are equal to unity.

CONCLUDING REMARKS

Finite difference solutions using the wave envelope concept are presented for plane wave sound propagation in a one-dimensional hard-wall duct and a two-dimensional soft-wall duct for zero Mach number. The results show the numerical procedure to be in agreement with the corresponding exact analytical results.

The wave envelope approach to the numerical problem reduces the number of grid points in the difference solution by one order of magnitude compared to the conventional difference technique. Because the wave envelope technique greatly reduces the required computer storage and solution time, it would be useful if the technique could be applied to skewed inlet pressure waves, varying area ducts, and ducts with axial variations in

impedance. However, the proper function accounting for the amplitude and axial periodicity must yet be developed for these more complicated problems.

Finally, the concept of an acoustic pressure diffusion boundary layer was introduced, and its role in sound propagation in ducts was discussed. In order to better illustrate this concept, the wave equation and boundary conditions are written such that the frequency no longer appears explicitly in them. The frequency effects in duct propagation can be visualized solely as an expansion and stretching of the suppressor duct.

Lewis Research Center,
National Aeronautics and Space Administration,
Cleveland, Ohio, April 23, 1974,
501-04.

APPENDIX A

SYMBOLS

A	coefficient matrix, eq. (73)
A_1	submatrix, eq. (74)
C	submatrix, eq. (74)
c	speed of sound
ΔdB	decrease in decibels
E	acoustic power, eq. (57)
\bar{F}	column vector, eq. (73)
f	frequency
f(x)	function of x
H	duct height, fig. 1
I	dimensionless intensity, eq. (54)
I'	dimensional intensity
i	$\sqrt{-1}$
L	dimensional length of duct, fig. 1
m	total number of grid rows (points in y-direction)
n	total number of grid columns (points in x-direction)
P	dimensionless pressure, $P(x,y) = P'/P'_A$
P'	dimensional pressure, $P'(x',y',t)$
P'_A	initial pressure amplitude at $x = 0$
P'_0	dimensional pressure, $P'_0(x',y')$
p	dimensionless pressure, eq. (20)
\bar{p}	dimensionless column pressure vector, eq. (73)
t	time
u	dimensionless acoustic particle velocity
u'	dimensional acoustic particle velocity, eq. (36)
X	dimensionless distance, eq. (76)

x dimensionless axial coordinate, eq. (4)
 Δx dimensionless axial grid spacing
 x' dimensional axial coordinate, fig. 1
 x_{eff} $x(H/L)$
 Y dimensional transverse coordinate, eq. (77)
 y dimensionless transverse coordinate, eq. (4)
 Δy dimensionless transverse grid spacing
 y' dimensional transverse coordinate, fig. 1
 Z acoustic impedance, eq. (39)
 δ acoustic pressure diffusion boundary layer thickness, fig. 11
 ζ dimensionless specific acoustic impedance
 η dimensionless frequency, eq. (6)
 η_{eff} $\eta(H/L)$
 θ dimensionless specific acoustic resistance, eq. (40)
 κ acoustic conductance ratio
 λ acoustic axial wavelength
 λ_1 wavelength of first radial mode, eq. (B5)
 ρ density
 σ acoustic susceptance ratio
 χ dimensionless specific acoustic reactance, eq. (40)
 ω circular frequency

Subscripts:

i, j axial and transverse indexes, respectively, fig. 4
 x axial direction
 y transverse direction

Superscripts:

$'$ dimensional quality
 $*$ complex conjugate
 $-$ vector quantity
 (1) real part
 (2) imaginary part

APPENDIX B

GENERALIZED WAVE ENVELOPE EQUATIONS

The Helmholtz equation (5), repeated here for convenience,

$$\frac{\partial^2 P}{\partial x^2} + \frac{\partial^2 P}{\partial y^2} + (2\pi\eta)^2 P = 0 \quad (\text{B1})$$

was transformed to a new form by assuming

$$P = pe^{-i2\pi\eta x} \quad (\text{B2})$$

where, as given in the body of the report (eq. (6)),

$$\eta = \frac{H}{\lambda} \quad (\text{B3})$$

The wavelength associated with the assumed transformation in equations (B2) and (B3) is

$$\lambda = \frac{c}{f} \quad (\text{B4})$$

This is the wavelength of a plane wave propagating in a hard-wall duct. Analytical theory (ref. 15) indicates that the wavelength of the first propagating radial (y or transverse) mode λ_1 in a soft-wall duct with an optimized acoustic impedance is approximately equal to the wavelength in a hard-wall duct; that is,

$$\lambda_1 \approx \lambda \quad (\text{B5})$$

This fact accounts for the good agreement between the numerical wave envelope theory and the analytical theory. Off-optimum impedances can be found for which equation (B5) is not a good approximation, and some ripple will probably result if the amplitude function given by equation (B2) is used. The plane input wave in a soft-wall duct consists of many higher order transverse modes, each with different λ 's; however, most of these modes carry very little energy (ref. 28, p. 308).

If higher order radial modes propagate through the duct (cut on), or if the inlet pressure profile is in the form of a higher order radial mode, the axial propagation

wavelength may be considerably different from the wavelength associated with hard-wall-duct propagation. For these cases, based on equations developed in the body of this report, the solution for the axial pressures may have large ripples. Although the governing differential equations are valid even if ripples are present, a sparse axial grid system will no longer lead to accurate predictions of pressure and acoustic intensity. Consequently, either the number of axial grid points must be increased or a better choice of λ must be made.

If a larger number of grid points is used, the wave envelope concept offers no real advantage over the standard finite difference technique presented in references 24 to 26. However, if the value of λ can be determined by an iteration technique, the wave envelope approach will still offer advantages.

If the input pressure wave is composed of two or more higher order radial modes which are equally important, it may not be possible to remove the pressure ripple. In this case, the analyst could use the standard difference technique of references 24 to 26, or he could Fourier decompose the inlet pressure wave into each of its radial components and treat each component separately by using the wave envelope concept. For the latter approach, the total intensity is composed of the intensity of the individual modes plus the coupling of energy between modes, as shown in reference 4.

REFERENCES

1. Morse, Philip M.: The Transmission of Sound Inside Pipes. *J. Acoust. Soc. Am.*, vol. 11, no. 2, Oct. 1939, pp. 205-210.
2. Cremer, Lothar: Theorie der Luftschall-Dämpfung in Rechteckkanal mit Schluckender Wand und das sich dabei Ergebende Hochste Dämpfungsmass. *Acustica*, vol. 3, no. 2, 1953, pp. 249-263.
3. Rice, Edward J.: Attenuation of Sound in Softwalled Circular Ducts. Presented at the AFOSR-UTIAS Symposium on Aerodynamic Noise, Toronto, May 20-21, 1968.
4. Rice, Edward J.: Propagation of Waves in an Acoustically Lined Duct with a Mean Flow. *Basic Aerodynamic Noise Research. NASA SP-207*, 1969, pp. 345-355.
5. Eversman, Walter: The Effect of Mach Number on the Tuning of an Acoustic Lining in a Flow Duct. *J. Acoust. Soc. Am.*, vol. 48, no. 2, pt. 1, 1970, pp. 425-428.
6. Tack, D. H.; and Lambert, R. F.: Influence of Shear Flow on Sound Attenuation in a Lined Duct. *J. Acoust. Soc. Am.*, vol. 38, no. 4, Oct. 1965, pp. 655-666.
7. Pridmore-Brown, D. C.: Sound Propagation in a Fluid Flowing Through an Attenuating Duct. *J. Fluid Mech.*, vol. 4, pt. 4, Aug. 1958, pp. 393-406.
8. Mungur, P.; and Gladwell, G. M. L.: Acoustic Wave Propagation in a Sheared Fluid Contained in a Duct. *J. Sound Vib.*, vol. 9, no. 1, Jan. 1969, pp. 28-48.
9. Mungur, P.; and Plumblee, H. E.: Propagation and Attenuation of Sound in a Soft-Walled Annular Duct Containing a Shear Flow. *Basic Aerodynamic Noise Research. NASA SP-207*, 1969, pp. 305-327.
10. Hersh, A. S.; and Catton, I.: Effect of Shear Flow on Sound Propagation in Rectangular Ducts. *J. Acoust. Soc. Am.*, vol. 50, no. 3, pt. 2, 1971, pp. 992-1003.
11. Eversman, Walter: Effect of Boundary Layer on the Transmission and Attenuation of Sound in an Acoustically Treated Circular Duct. *J. Acoust. Soc. Am.*, vol. 49, no. 5, pt. 1, 1971, pp. 1372-1380.
12. Mariano, S.: Effect of Wall Shear Layers on the Sound Attenuation in Acoustically Lined Rectangular Ducts. *J. Sound Vib.*, vol. 19, no. 3, Dec. 8, 1971, pp. 261-275.
13. Savkar, S. D.: Propagation of Sound in Ducts with Shear Flow. *J. Sound Vib.*, vol. 19, no. 3, Dec. 8, 1971, pp. 355-372.
14. Shankar, P. N.: On Acoustic Refraction by Duct Shear Layers. *J. Fluid Mech.*, vol. 47, pt. 1, May 14, 1971, pp. 81-91.

15. Rice, E. J.: Performance of Noise Suppressors for a Full-Scale Fan For Turbofan Engines. Paper 71-1-183, 1971.
16. Ko, S. -H.: Sound Attenuation in Acoustically Lined Circular Ducts in the Presence of Uniform Flow and Shear Flow. J. Sound Vib., vol. 22, no. 2, May 22, 1972, pp. 193-210.
17. Shankar, P. N.: Sound Propagation in Duct Shear Layers. J. Sound Vib., vol. 22, no. 2, May 22, 1972, pp. 221-232.
18. Shankar, P. N.: Acoustic Refraction and Attenuation in Cylindrical and Annular Ducts. J. Sound Vib., vol. 22, no. 2, May 22, 1972, pp. 233-246.
19. Huerre, P.; and Karamcheti, K.: Propagation of Sound Through a Fluid Moving in a Duct of Varying Area. In Interagency Symposium on University Research in Transportation Noise, Stanford University, vol. II, Mar. 28-30, 1973, pp. 397-413.
20. King, L. S.; and Karamcheti, K.: Propagation of Plane Waves in the Flow Through a Variable Area Duct. Paper 73-1009, AIAA, Oct. 1973.
21. Nayfeh, A. H.; Telionis, D. P.; and Lekoudas, S. G.: Acoustic Propagation in Ducts with Varying Cross Sections and Sheared Mean Flow. Paper 73-1008, AIAA, Oct. 1973.
22. Beckemeyer, R. J.; and Eversman, W.: Computational Methods for Studying Acoustic Propagation in Nonuniform Waveguides. Paper 73-1006, AIAA, Oct. 1973.
23. Eversman, W.: The Transmission of Sound in Nonuniform Ducts. In Interagency Symposium on University Research in Transportation Noise. Stanford University, vol. II, Mar. 28-30, 1973, pp. 414-429.
24. Baumeister, Kenneth J.; and Bittner, Edward C.: Numerical Simulation of Noise Propagation in Jet Engine Ducts. NASA TN D-7339, 1973.
25. Baumeister, Kenneth J.; and Rice, Edward J.: A Difference Theory for Noise Propagation in an Acoustically Lined Duct with Mean Flow. Paper 73-1006, AIAA, Oct. 1973.
26. Baumeister, Kenneth J.: Application of Finite Difference Techniques to Noise Propagation in Jet Engine Duct. Paper 73-WA/GT-10, 1973.
27. McCormick, John M.; and Salvador, Mario G.: Numerical Methods in FORTRAN. Prentice-Hall, 1964.
28. Morse, Philip M.: Vibration and Sound. 2nd ed., McGraw-Hill, 1948.

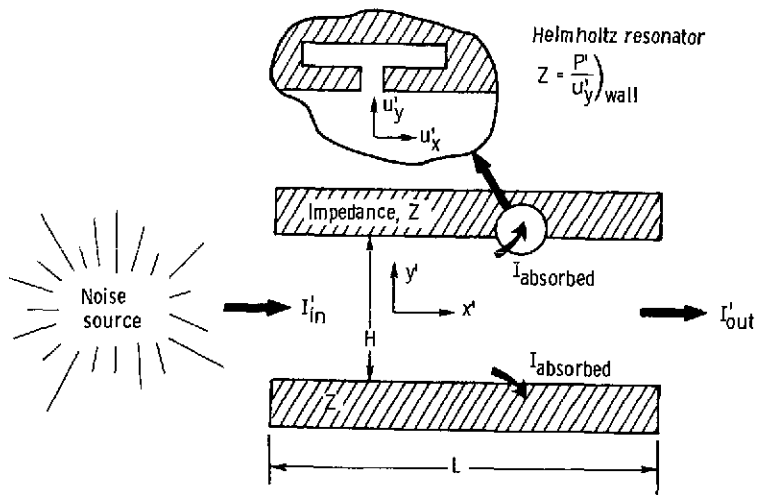


Figure 1. - Schematic of turbojet suppressor duct using a Helmholtz resonator.

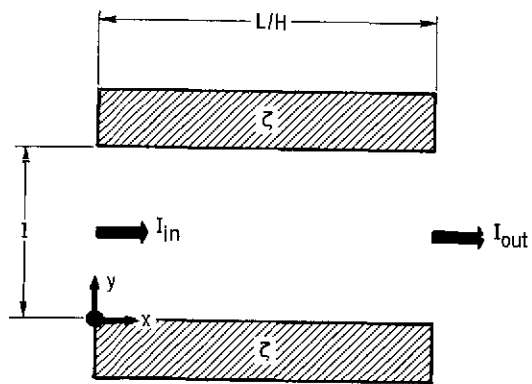


Figure 2. - Dimensionless (scaled) Cartesian coordinate system for suppressor duct.

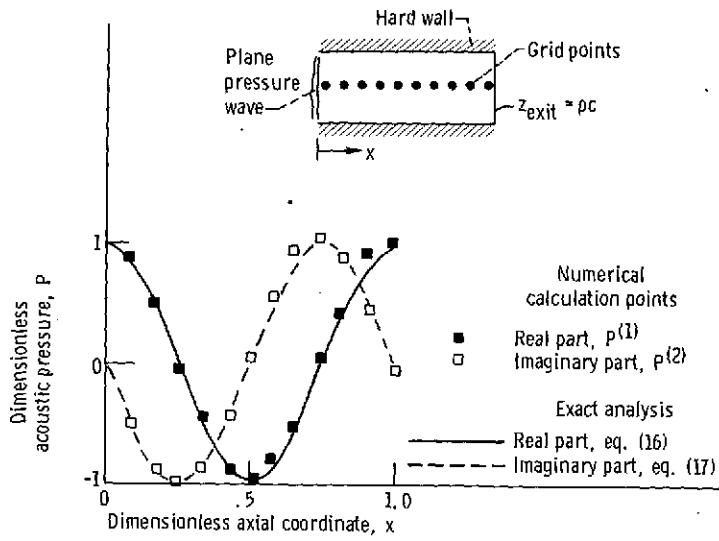


Figure 3. - Analytical and numerical pressure profiles for one-dimensional sound propagation in hard-wall duct. Dimensionless frequency $\eta = 1$. $P = p^{(1)} + ip^{(2)}$.

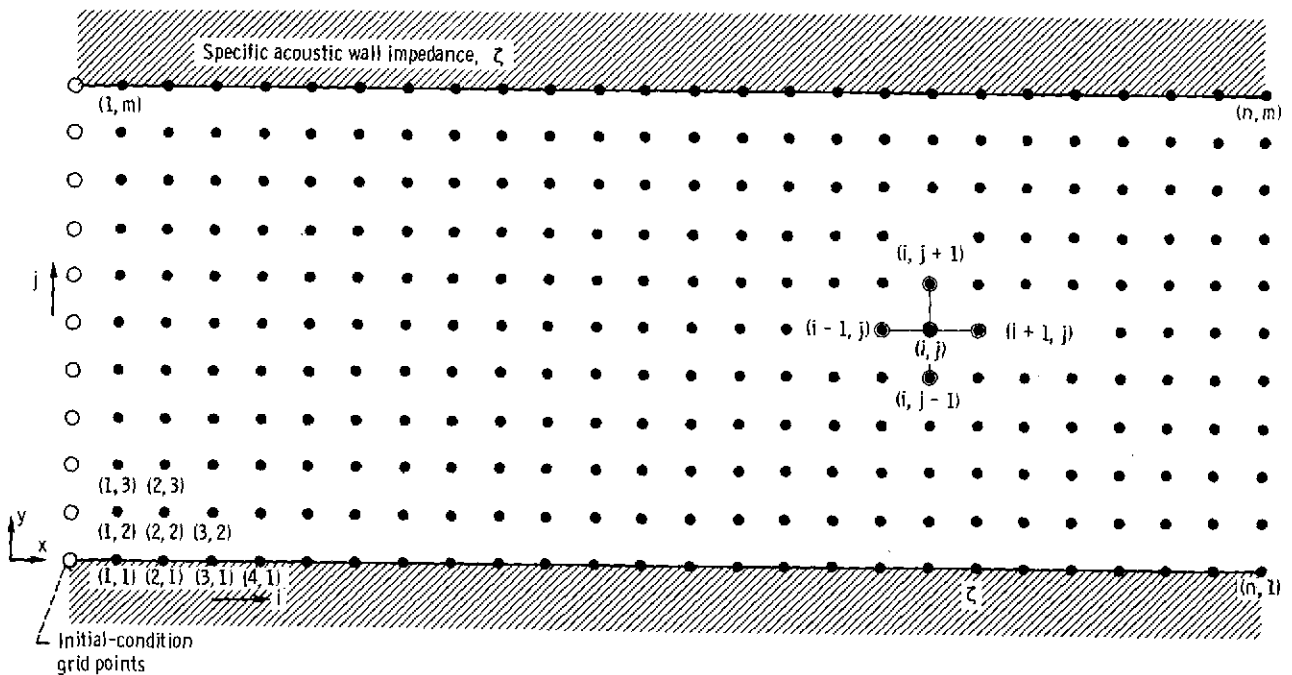


Figure 4. - Grid-point representation of two-dimensional flow duct.

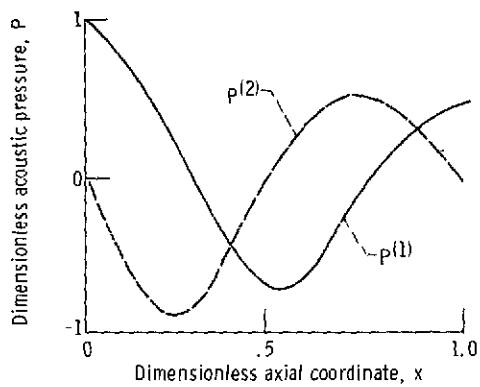


Figure 5. - Typical pressure profile for sound propagation in a soft-wall duct for dimensionless frequency $\eta = 1$ and duct length $L/H = 1$.

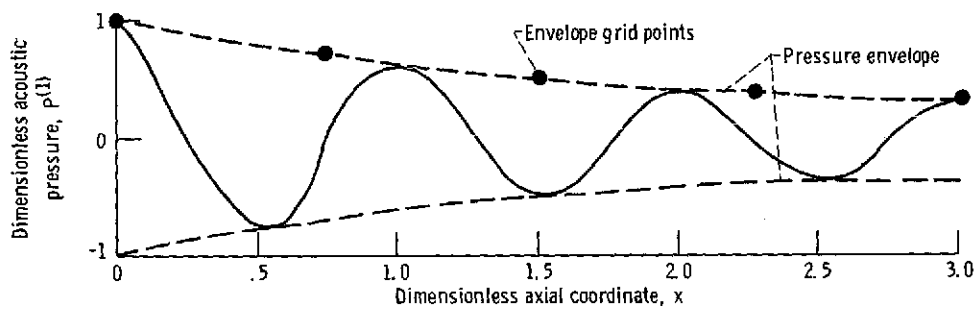


Figure 6. - Typical pressure profile for sound propagation in a soft-wall duct for dimensionless frequency $\eta = 1$ and duct length $L/H = 3$.

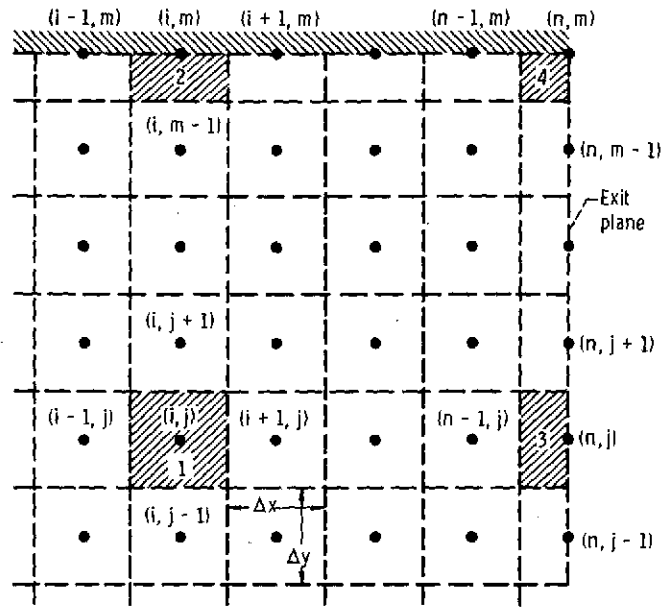


Figure 7. - Integration cells for establishing difference equations.

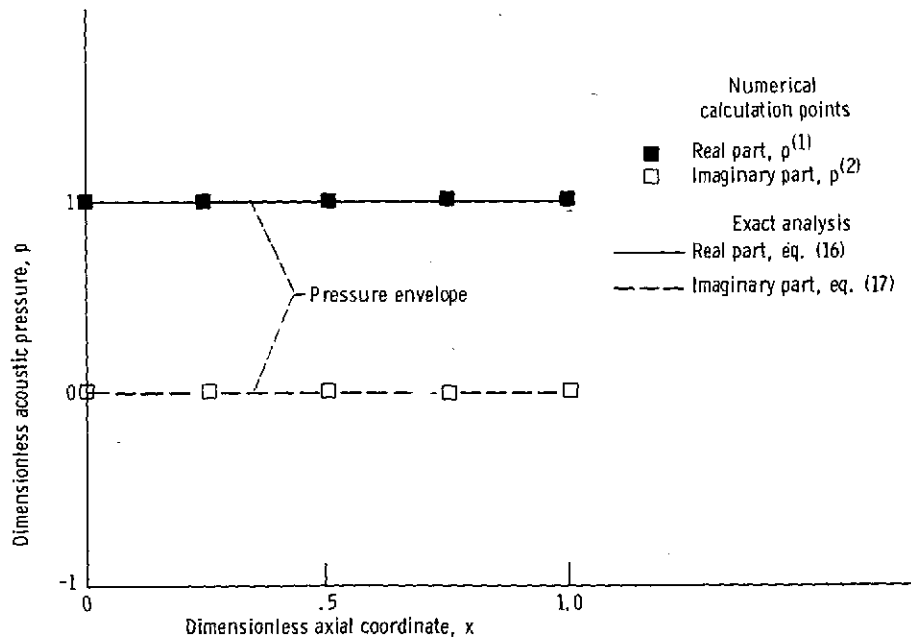


Figure 8. - Analytical and numerical dimensionless acoustic pressure profiles for sound propagation in a hard-wall duct. Dimensionless frequency $\eta = 1$; number of grid columns $n = 4$; $p = p^{(1)} + ip^{(2)}$.

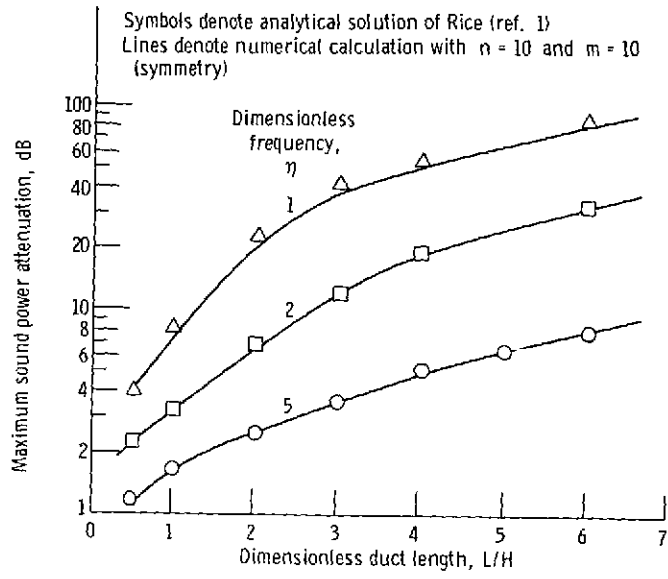


Figure 9. - Effect of axial length and frequency on attenuation at optimum impedance in two-dimensional duct.

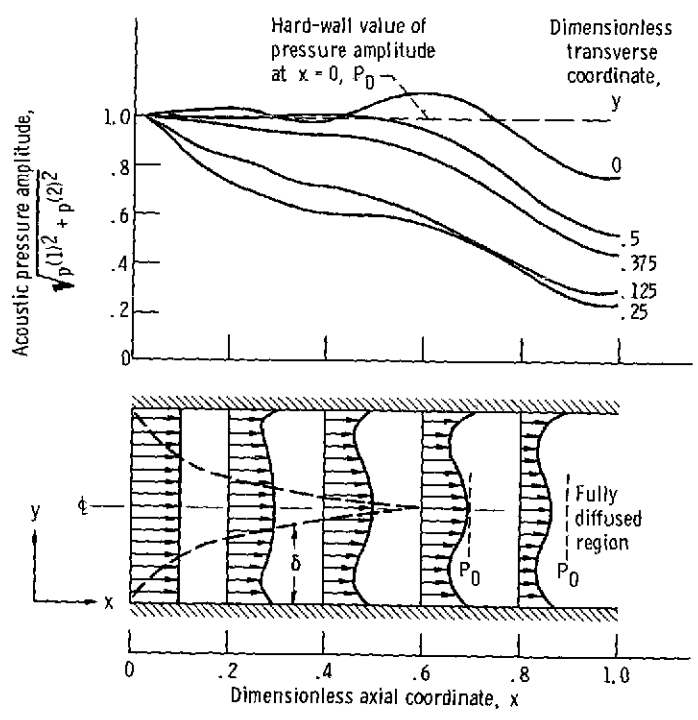
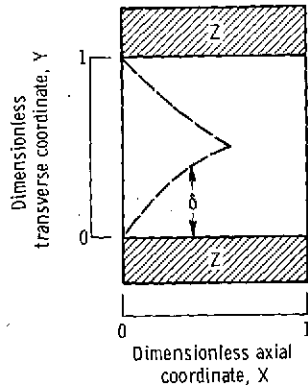
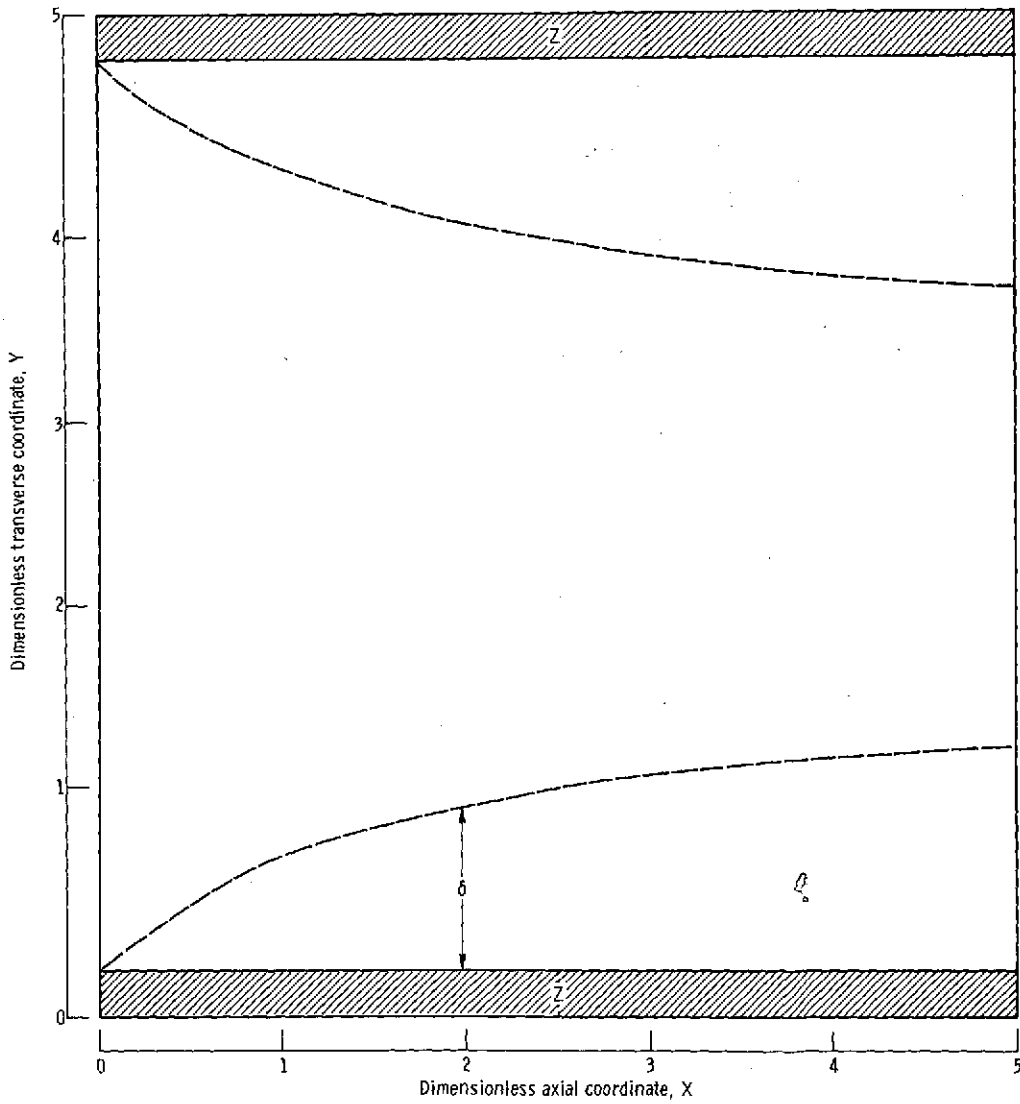


Figure 10. - Pressure amplitude fluctuations along duct at optimum impedance for dimensionless frequency $\eta = 1$, dimensionless duct length $L/H = 1$, number of grid rows $m = 10$, and number of grid columns $n = 10$.

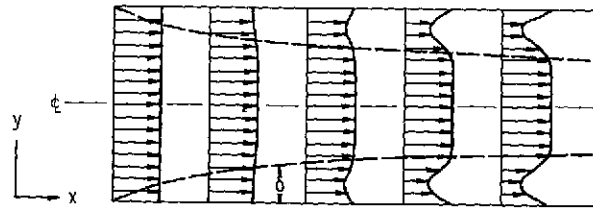
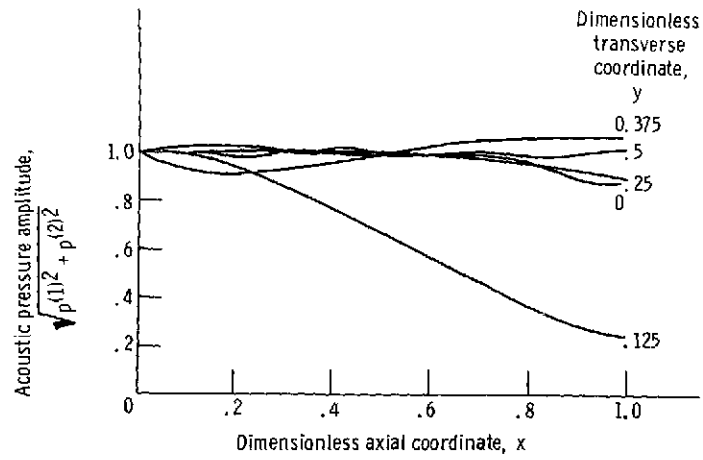


(a) Dimensionless frequency $\eta = 1$.

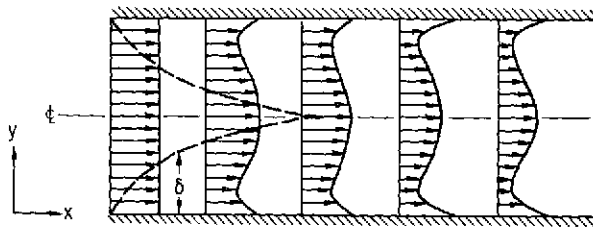
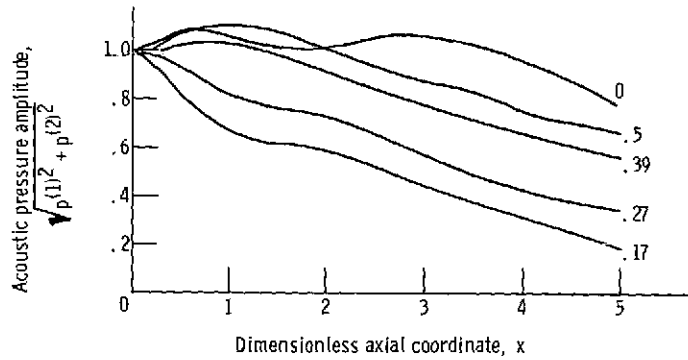


(b) Dimensionless frequency $\eta = 5$.

Figure 11. - Effect of dimensionless frequency on relative size of suppressor duct in X-Y coordinates for constant duct height and a dimensionless duct length $L/H = 1$ for optimum acoustic impedance.



(a) Dimensionless duct length $L/H = 1$.



(b) Dimensionless duct length $L/H = 5$.

Figure 12. - Pressure amplitude variations along duct at optimum impedance for dimensionless frequency $\eta = 5$ with number of grid rows $m = 10$ (symmetry boundary) and number of grid columns $n = 10$.

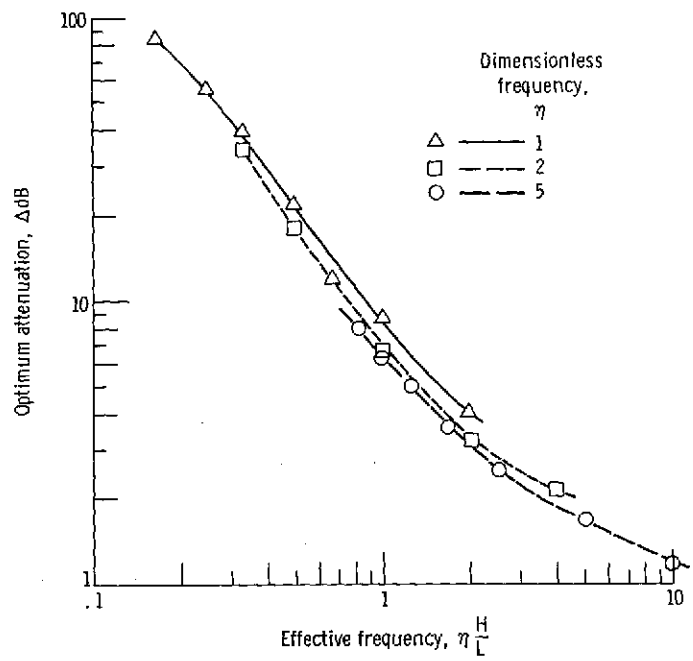


Figure 13. - Relation between optimum attenuation and effective frequency.